nature structural & molecular biology

N-linked glycosylation of SV2 is required for binding and uptake of botulinum neurotoxin A

Guorui Yao[1,9], Sicai Zhang[2–4,9], Stefan Mahrhold[5,9], Kwok-ho Lam[1], Daniel Stern[6], Karine Bagramyan[7], Kay Perry[8], Markus Kalkum[7], Andreas Rummel[5], Min Dong[2–4] & Rongsheng Jin[1]

Botulinum neurotoxin serotype A1 (BoNT/A1), a licensed drug widely used for medical and cosmetic applications, exerts its action by invading motoneurons. Here we report a 2.0-Å-resolution crystal structure of the BoNT/A1 receptor-binding domain in complex with its neuronal receptor, glycosylated human SV2C. We found that the neuronal tropism of BoNT/A1 requires recognition of both the peptide moiety and an N-linked glycan on SV2. This N-glycan—which is conserved in all SV2 isoforms across vertebrates—is essential for BoNT/A1 binding to neurons and for its potent neurotoxicity. The glycan-binding interface on SV2 is targeted by a human BoNT/A1-neutralizing antibody currently licensed as an antibotulism drug. Our studies reveal a new paradigm of host-pathogen interactions, in which pathogens exploit conserved host post-translational modifications, thereby achieving highly specific receptor binding while also tolerating genetic changes across multiple isoforms of receptors.

BoNT/A1 is one of the seven major serotypes of BoNT (termed BoNT/A–G). According to a well-accepted dual-receptor model, the high potency of BoNT/A1 targeting motoneurons is mediated by its receptor-binding domain (H_CA), which synergistically binds host protein receptors and gangliosides on the neuronal surface at neuromuscular junctions[1–3]. The synaptic vesicle glycoprotein 2 (SV2), a family of 12-transmembrane-domain proteins including three isoforms (SV2A, SV2B, and SV2C) in mammals, are protein receptors for BoNT/A1 (refs. 4,5) as well as for BoNT/E[6], BoNT/D[7], and potentially BoNT/F[8,9].

We have previously mapped the BoNT/A1-binding site to the fourth luminal domain of SV2 (SV2-L4)[4,5]. A crystal structure of H_CA in complex with the recombinant human SV2C-L4 expressed in *Escherichia coli* (referred to as bSV2C, with 'b' indicating bacterial expression) has recently been reported[10]. This structure shows that H_CA-bSV2C recognition relies mostly on backbone-to-backbone interactions within a small interface (~596 Å^2), mediated by two β-strands in H_CA and one open edge of the quadrilateral β-helices of bSV2C[10]. This binding mode is in sharp contrast to that of BoNT/B, which recognizes its receptors, synaptotagmin-I and synaptotagmin-II (Syt-I/II), through an extensive side chain–mediated protein-protein-interaction network that ensures high binding affinity and specificity toward Syt-I/II[11,12]. These findings prompt the question of how BoNT/A1 achieves its high efficacy of targeting neurons through receptor recognition based primarily on backbone-mediated interactions.

To better understand the molecular mechanism underlying BoNT/A1's extraordinary neuronal tropism, we determined the crystal structures of H_CA in complex with rat bSV2C-L4 and the physiologically more relevant glycosylated human SV2C-L4. We found that BoNT/A1 recognizes two distinct structural elements on SV2C: the protein moiety and an N-linked glycan that is conserved in all known SV2 homologs across vertebrates. Further biophysical, cellular, and functional studies demonstrated that SV2 glycans are essential for BoNT/A1 binding to neurons and for its extreme toxicity at its physiological site of action, the motor nerve terminals. Moreover, we found that the glycan-binding site of BoNT/A1 is also the target of a potent human neutralizing antibody, thus suggesting the potential for SV2 glycan as a new target for the development of BoNT inhibitors.

RESULTS

The crystal structure of H_CA in complex with rat bSV2C

Amino acid sequence analyses showed that even the few residues that mediate side chain interactions in the H_CA and human bSV2C complex are not strictly conserved in SV2A and SV2B, or even SV2C from other species (for example, rodents) (**Supplementary Note 1**). To gain better insight into how BoNT/A1 recognizes SV2C from different species, we determined the crystal structure of H_CA in complex with rat SV2C-L4 expressed in *E. coli* (**Table 1**). The structure of the rat bSV2C–H_CA complex is virtually identical to that of the human bSV2C complex (r.m.s. deviation of ~0.70 Å over 496 aligned Cα pairs). We observed

[1]Department of Physiology and Biophysics, University of California, Irvine, Irvine, California, USA. [2]Department of Urology, Boston Children's Hospital, Harvard Medical School, Boston, Massachusetts, USA. [3]Department of Microbiology and Immunobiology, Harvard Medical School, Boston, Massachusetts, USA. [4]Department of Surgery, Harvard Medical School, Boston, Massachusetts, USA. [5]Institut für Toxikologie, Medizinische Hochschule Hannover, Hannover, Germany. [6]Centre for Biological Threats and Special Pathogens–Biological Toxins (ZBS3), Robert Koch-Institut, Berlin, Germany. [7]Department of Molecular Immunology, Beckman Research Institute of City of Hope, Duarte, California, USA. [8]NE-CAT, Argonne National Laboratory, Department of Chemistry and Chemical Biology, Cornell University, Argonne, Illinois, USA. [9]These authors contributed equally to this work. Correspondence should be addressed to R.J. (r.jin@uci.edu), M.D. (min.dong@childrens.harvard.edu) or A.R. (rummel.andreas@mh-hannover.de).

Received 16 March; accepted 13 May; published online 13 June 2016; doi:10.1038/nsmb.3245

Table 1 Data collection and refinement statistics

	H_CA–bSV2C (PDB 5JMC)	H_CA–gSV2C (PDB 5JLV)
Data collection		
Space group	$P12_11$	$C121$
Cell dimensions		
a, *b*, *c* (Å)	88.66, 143.99, 110.92	109.00, 111.85, 126.25
α, *β*, *γ* (°)	90, 93.6, 90	90, 101.3, 90
Resolution (Å)	87.76–2.64 (2.73–2.64)[a]	123.81–2.00 (2.03–2.00)
R_{meas}	0.172 (1.454)	0.159 (0.889)
$I/\sigma(I)$	9.09 (1.43)	6.7 (2.1)
$CC_{1/2}$	0.991 (0.599)	0.984 (0.722)
Completeness (%)	99.4 (99.2)	99.6 (99.9)
Redundancy	3.4 (3.1)	2.9 (2.9)
Refinement		
Resolution (Å)	87.76–2.64	123.81–2.00
No. reflections	80,958	99,659
R_{work} / R_{free}	0.239 / 0.275	0.175 / 0.216
No. atoms		
Protein	16,825	8,641
Ligand	–	128
Water	162	659
B factors		
Protein	58.50	44.50
Ligand	–	58.70
Water	55.40	51.50
R.m.s. deviations		
Bond lengths (Å)	0.012	0.009
Bond angles (°)	1.22	1.01

One crystal was used for each structure. [a]Values in parentheses are for the highest-resolution shell.

two major differences. First, H_CA R1294 forms hydrogen bonds with S519, C520, T521, and D539 of rat bSV2C (**Supplementary Fig. 1**), but these bonds are not present in the structure of the human bSV2C–H_CA complex, probably because of the different crystal-packing modes[10]. Interestingly, R1294 exists in only two of the eight BoNT/A subtypes currently known (BoNT/A1 and A4). Second, a cation-π stacking interaction between BoNT/A1 R1156—a residue present exclusively in subtype BoNT/A1—and human SV2C F563, which is thought to be critical for BoNT/A1-SV2C recognition[10], is not present in the rat bSV2C–H_CA complex because rat SV2C has a leucine (L563) in place of human SV2C F563. Leucine is also the homologous residue on SV2A and SV2B in both humans and rodents (**Supplementary Note 1**). These findings suggest that side chain–mediated interactions may vary substantially among different BoNT/A subtypes and SV2 isoforms and thus are unlikely to provide sufficient binding specificity and affinity between BoNT/A and SV2. Therefore, some crucial BoNT/A-SV2 interactions are missing in the crystal structures of the H_CA–bSV2C complexes described here and previously[10].

SV2 glycosylation is crucial for BoNT/A1 binding to neurons

Native SV2s are glycosylated in neurons[13], and one of the three N-linked-glycosylation motifs in L4—which is conserved in all SV2 isoforms across vertebrates—is located at the center of the BoNT/A1-binding interface of SV2 (for example, N573 in SV2A, N516 in SV2B, and N559 in SV2C in humans) (**Supplementary Note 1**). To explore the functional role of this N-linked glycan, we used a molecular replacement approach to express either wild type (WT) SV2A–C or the corresponding deglycosylation mutants (SV2A N573A, SV2B N516A, and SV2C N559A) in hippocampal and cortical neurons cultured from SV2A/SV2B double-knockout (KO) mice. Most hippocampal and cortical neurons do not express SV2C[13], and thus these neurons cultured from SV2A/SV2B double-KO mice served as an SV2-null neuron model. These deglycosylation mutations of SV2 do not affect protein-protein interactions with BoNT/A1; for example, bSV2C N559A maintains WT-like binding to H_CA[10].

The deglycosylation mutants of SV2A–C all showed lower molecular weights than those of WT SV2s, thus confirming that this asparagine residue is indeed glycosylated in neurons (**Fig. 1a**,**b** and **Supplementary Fig. 2**). The expression level of SV2A N573A was comparable to that of WT SV2A, but there was a drastic decrease in SV2B N516A expression and a mild decrease in SV2C N559A expression (**Supplementary Fig. 2**). These results suggest that glycosylation

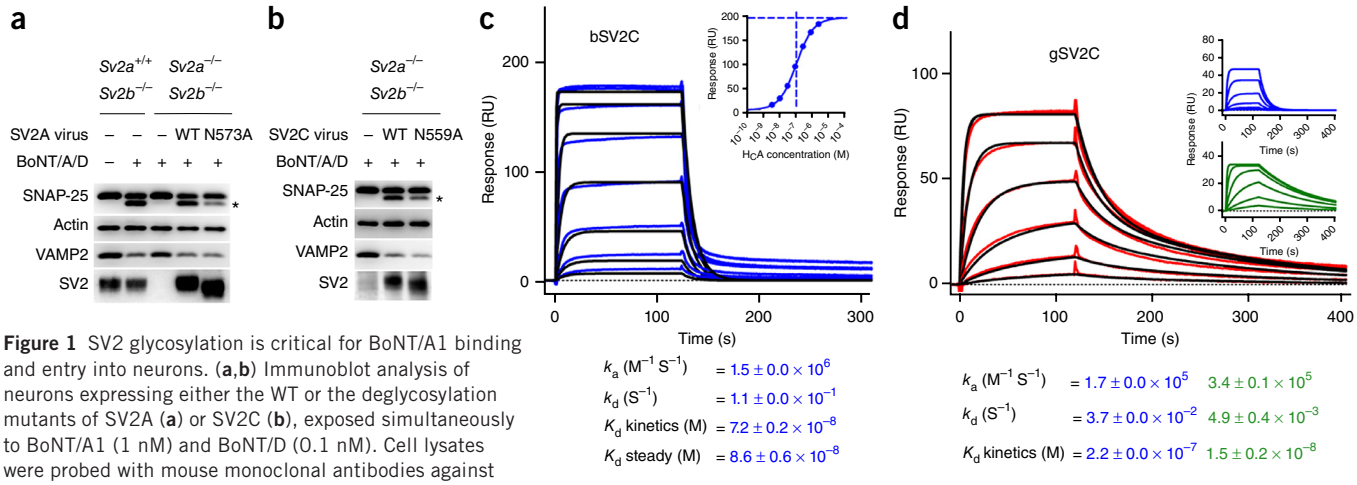

Figure 1 SV2 glycosylation is critical for BoNT/A1 binding and entry into neurons. (**a**,**b**) Immunoblot analysis of neurons expressing either the WT or the deglycosylation mutants of SV2A (**a**) or SV2C (**b**), exposed simultaneously to BoNT/A1 (1 nM) and BoNT/D (0.1 nM). Cell lysates were probed with mouse monoclonal antibodies against SNAP-25 (Cl 71.2), VAMP2 (Cl 69.1), and SV2 (pan-SV2). BoNT/D is an internal control to confirm correct sorting and localization of SV2 mutants. Asterisk, smaller fragment generated by cleavage of SNAP-25 by BoNT/A1. β-actin is a loading control. Uncropped blot images are shown in **Supplementary Data Set 1**. (**c**) SPR sensorgrams of H_CA binding to immobilized human bSV2C (blue) overlaid with a fit of 1:1 binding model (black). Because equilibrium binding was reached for all conditions tested, a steady-state affinity was also determined (inset). RU, resonance units. (**d**) H_CA binding to immobilized human gSV2C (red). The binding was best fit to a heterogeneous binding model (black), whereas a 1:1 binding model was inapplicable. Inset, individual contributions of the two binding events observed in the heterogeneous interaction (blue and green). Shown values are means ± s.d. (from 2 or 3 independent experiments for bSV2C and gSV2C, respectively).

at this site is crucial for the folding and/or stability of SV2B and to a lesser degree SV2C, consistently with previously described functions of N-linked glycans[14].

We thus focused on SV2A N573A and SV2C N559A, and examined SV2-mediated toxin entry for BoNT/A1 and BoNT/D by analyzing the cleavage of synaptosomal-associated protein of 25 kDa (SNAP-25, the substrate of BoNT/A1) and synaptobrevin/vesicle-associated membrane protein 2 (VAMP2, the substrate of BoNT/D) after toxin exposure. BoNT/D served as an internal control for regular trafficking and sorting of SV2 mutants, because BoNT/D uses SV2s as receptors independently of N-glycosylation[7]. Furthermore, we have previously shown that BoNT/B, which does not use SV2 as its receptor, binds and enters WT and SV2-KO neurons to similar extents[4,6]. We found that the SV2-KO neurons did not show BoNT/A1 entry at the conditions tested, probably because of BoNT/A1's low affinity for the ganglioside receptor, which is unable to allow BoNT/A1 cell entry in the absence of SV2 (refs. 15,16). Expression of SV2A N573A and SV2C N559A mediated substantially less entry of BoNT/A1 than did the WT SV2s, whereas BoNT/D entry was not affected (**Fig. 1a**,**b**). These results suggest that SV2 glycosylation at this strictly conserved site contributes to BoNT/A1 binding and entry into neurons.

SV2C glycans greatly enhance H_CA binding

Glycosylation is a common and highly diverse post-translational protein modification that profoundly alters protein behavior[14]. Do the N-glycans directly contribute to BoNT/A1 binding? To answer this question, we first carried out surface plasmon resonance (SPR) analysis to examine how H_CA binds to human bSV2C. We found that the binding displayed a fast association rate (k_a of 1.5×10^6 M^{-1} s^{-1}) and a fast dissociation rate (k_d of 0.11 s^{-1}) (**Fig. 1c**), and the overall dissociation constant (K_d) of ~86 nM was comparable to a previously reported K_d of 260 nM determined by fluorescence anisotropy[10]. The nature of this transient interaction is consistent with the pattern of backbone-to-backbone interactions revealed in the crystal structure but is difficult to reconcile with the extremely high specificity of BoNT/A1 toward neurons.

We then expressed the human SV2C-L4 (residues V473–T567) as a secreted protein in human embryonic kidney 293 cells (HEK293) to mimic the physiologically relevant glycosylated receptor. HEK293 cells have been widely used to produce glycoproteins with human glycosylation patterns[17]. The resulting protein (referred to as gSV2C, in which 'g' stands for glycosylation) is glycosylated, as evidenced by the appearance of multiple SDS–PAGE bands with masses larger than its peptide mass, comprising heterogeneous glycoforms. We characterized binding of H_CA to gSV2C by SPR, which revealed two binding components (**Fig. 1d**). A transient low-affinity binding (K_d of ~220 nM) closely resembled the binding of H_CA to bSV2C, probably because of heterogeneous glycosylation of SV2C under overexpression conditions[18]. Notably, high-affinity binding (K_d of ~15 nM) of gSV2C displayed a ~22-fold slower dissociation rate and an ~4-fold slower association rate than bSV2C. The slightly decreased association rate of gSV2C is likely to stem from restricted carbohydrate flexibility after toxin binding, a physiological event encountered by BoNT/A1 *in vivo* because the neuronal SV2s are glycosylated. Therefore, the relatively fast association rate displayed by bSV2C artificially increased the binding affinity of bSV2C. Together, these data demonstrate that the glycans of gSV2C stabilize the H_CA–gSV2C complex by markedly decreasing the dissociation rate.

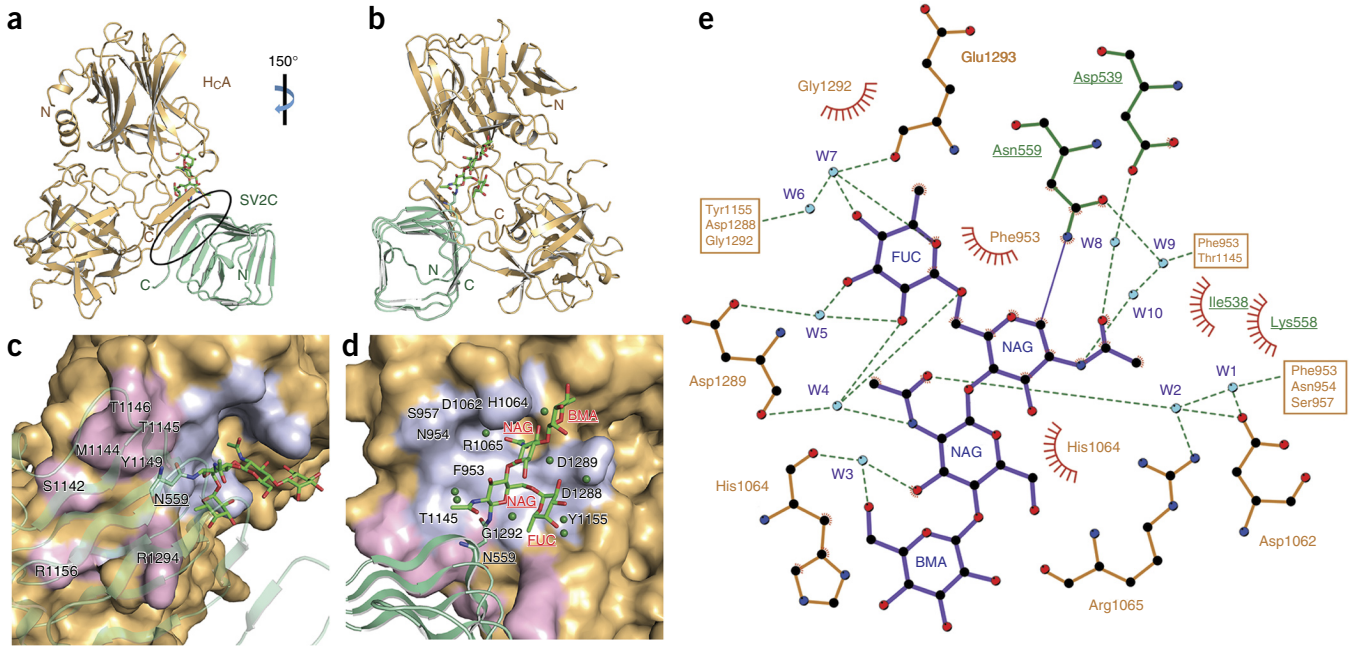

Figure 2 Structure of H_CA in complex with human gSV2C. (**a**) Cartoon representation of the complex, with H_CA in gold, gSV2C in green, and a black oval highlighting the interacting β-strands between them. gSV2C N559 and the attached N-linked glycan are shown in stick models. (**b**) An ~150° rotation of the complex about a vertical axis. (**c**,**d**) Close-up views of the protein-protein (**c**) and protein-glycan (**d**) association interfaces between H_CA and gSV2C. H_CA is in surface representation (gold), and H_CA residues that directly interact with the peptide moiety of gSV2C or the N559 glycan are purple and light blue, respectively. gSV2C N559 and the N-linked glycan are labeled as black and red underlined text, respectively. Well-defined water molecules that mediate H_CA-glycan binding are shown as green spheres. (**e**) Extensive interactions between gSV2C N559 glycan and H_CA. The plots were generated with LIGPLOT[36]. H_CA and gSV2C residues are brown and green, respectively. Hydrogen bonds are indicated by dashed green lines. Key hydrogen-bonding distances are listed in **Supplementary Table 1**. Residues involved in hydrophobic interactions are represented by an arc with spokes radiating toward the binding partners that they contact. W1 to W10 correspond to the following waters in PDB 5JLV: A1545, A1484, C712, A1476, C711, A1475, A1445, C729, A1485, and C701.

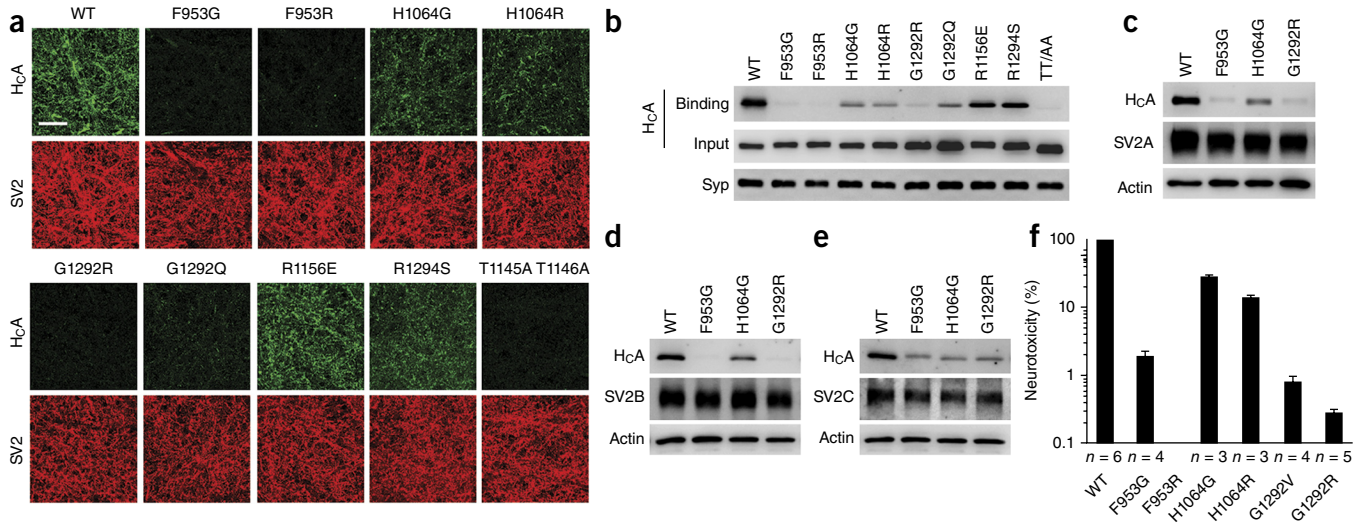

Figure 3 Site-directed-mutagenesis analysis of the SV2-binding site on H_CA. (**a**,**b**) Binding of H_CA variants (100 nM) to rat hippocampal and cortical neurons, analyzed by immunostaining (**a**) or immunoblotting (**b**). Scale bar in **a**, 20 µm. Synaptophysin (Syp) is a loading control in **b**. TT/AA, T1145A T1146A. (**c**–**e**) Immunoblot analysis of binding of H_CA variants (100 nM) to neurons expressing SV2A (**c**), SV2B (**d**), or SV2C (**e**). β-actin is a loading control. The corresponding immunostaining analyses are shown in **Supplementary Figure 6**. Uncropped blot images are shown in **Supplementary Data Set 1**. (**f**) MPN assay showing drastically decreased neurotoxicity of glycan-binding-deficient BoNT/A1. Graph shows means ± s.d. of *n* technical replicates; *n* values are shown below each bar. Source data are available online.

The crystal structure of H_CA in complex with human gSV2C

We next determined the crystal structure of H_CA in complex with human gSV2C at 2.0-Å resolution (**Table 1**). The overall architecture of the H_CA–gSV2C complex is similar to that of the bSV2C complex (r.m.s. deviation of ~0.88 Å over 489 aligned Cα pairs). We observed a complex-type N-linked glycan attached to gSV2C N559, with clear electron densities for the quadruple-saccharide core made up of two *N*-acetylglucosamines (NAGs), a mannose (BMA), and a fucose (FUC) (**Fig. 2** and **Supplementary Fig. 3**). Two other putative N-linked-glycosylation sites (N484 and N534) are localized on SV2C-L4 and also conserved on SV2A and SV2B (**Supplementary Note 1**). We observed only one NAG resolved in the electron density for the N534 glycan, probably because of its high mobility, whereas we identified no sugar at N484. SV2C N484 and N534 are located far away from BoNT/A1-binding interface and thus are unlikely to directly participate in toxin binding.

Remarkably, the N559 glycan directly interacts with H_CA through a network of hydrogen bonds and van der Waals contacts. The most prominent interactions are stacking interactions between residues F953 and H1064 of H_CA and the hydrophobic faces of the two NAGs. In addition, ten well-defined water molecules act as molecular 'glue' in the glycan-H_CA interface, thus further strengthening the interactions (**Fig. 2d**,**e** and **Supplementary Table 1**). These interactions almost double the contact area between H_CA and SV2C from 557 Å^2 to 925 Å^2. There are also weak electron densities beyond the mannose, thus suggesting that there might be more extensive H_CA-glycan interactions that were not resolved, possibly because of the inherent flexibility of glycans and heterogeneous glycosylation. This structure unambiguously reveals that the N559 glycan of SV2C is recognized directly by BoNT/A1 as an integral part of the toxin-binding site.

SV2 glycan is critical for BoNT/A1 binding to neurons

We then sought to understand the functional role of protein-glycan interactions in BoNT/A1-SV2 recognition. On the basis of the crystal structure, we designed a set of single-site mutations on H_CA that selectively disrupt glycan binding: F953G and H1064G abolish the critical stacking of aromatic side chains against the sugar rings, and F953R, H1064R, G1292Q, and G1292R cause clashes between their bulky side chains and the N559 glycan. None of these mutations affected H_CA folding and stability, as verified by thermal denaturation experiments, nor did they affect H_CA binding to bSV2C, as demonstrated by pulldown and SPR studies. As expected, these mutants markedly decreased H_CA binding to gSV2C, a result strongly supporting the direct involvement of the N559 glycan of SV2C in BoNT/A1 binding (**Supplementary Figs. 4** and **5a**–**c**). Interestingly, SPR studies showed that the glycan-binding-deficient H_CA F953G bound much more weakly to gSV2C than to bSV2C (K_d values of ~760 nM and ~160 nM, respectively) (**Supplementary Fig. 5d**,**e**). Therefore, the native neuronal SV2s that are always glycosylated initially impose steric hindrances in BoNT/A1 recognition. However BoNT/A1 overcomes this obstacle by directly using SV2 glycans to strengthen binding.

We examined how these H_CA mutants bind to native SV2s in neurons. First, we analyzed binding of H_CA to endogenous SV2A and SV2B by using cultured rat hippocampal and cortical neurons[13] (**Fig. 3a**,**b**). The mutations F953G, F953R, G1292Q, and G1292R largely abolished binding of H_CA to neurons; H1064G and H1064R also drastically decreased binding, thus suggesting that protein-glycan interactions are essential for BoNT/A1 binding to native SV2s on neurons. We further examined neurons that exclusively expressed SV2A, SV2B, or SV2C: hippocampal and cortical neurons cultured from $Sv2a^{+/+}Sv2b^{-/-}$ mice served as neurons that express only SV2A, and we created neurons that expressed only SV2B or SV2C by infecting neurons cultured from $Sv2a^{-/-}Sv2b^{-/-}$ mice with lentiviruses for expression of SV2B or SV2C, respectively. Mutating glycan-binding residues on H_CA (for example, F953G, G1292R, and H1064G) decreased H_CA binding in all cases tested, thus demonstrating that BoNT/A1-glycan interactions are conserved and are essential for all three SV2 isoforms (**Fig. 3c**–**e** and **Supplementary Fig. 6**).

SV2 glycan allows tolerance to genetic changes in BoNT/A

Complementing our studies on protein-glycan interactions, we also examined the contribution of side chain–mediated protein-protein

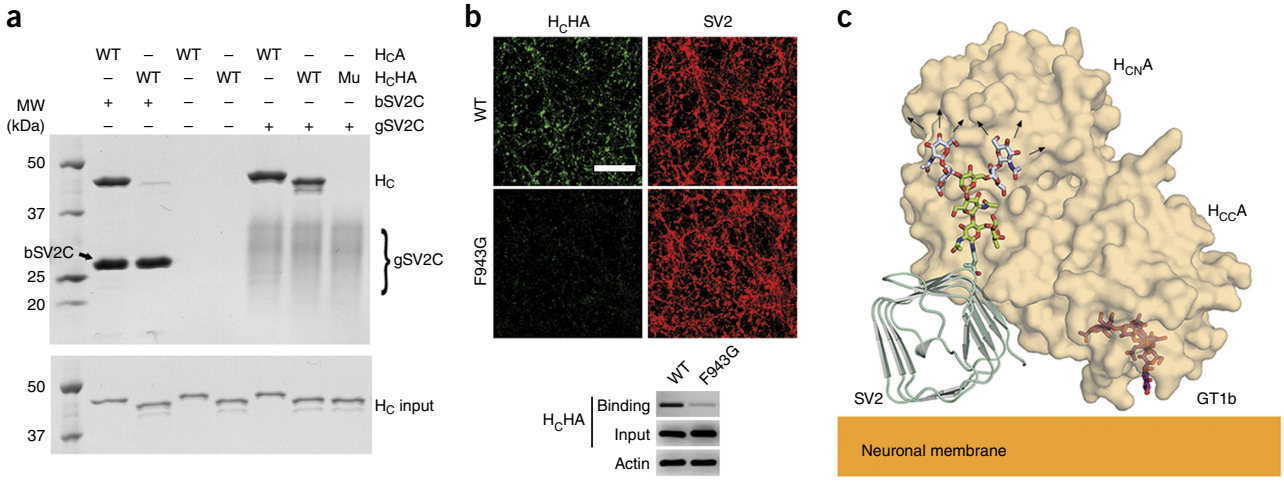

Figure 4 The SV2 glycan binding mode is conserved in BoNT/HA. (**a**) Pulldown assays demonstrating the indispensable role of SV2C glycan in H_CHA binding. Human bSV2C (with a SUMO tag) or gSV2C were used as baits. Mu, H_CHA F943G mutant; MW, molecular weight. (**b**) Immunostaining and immunoblotting analyses showing decreased binding of H_CHA F943G to rat cortical neurons. Uncropped images of gels and blots are shown in **Supplementary Data Set 1**. (**c**) Proposed model for simultaneous binding of BoNT/A1 to two neuronal surface receptors: glycosylated SV2 and ganglioside. GT1b is modeled on the basis of the structure of a GT1b-bound H_CA (PDB 2VU9)[37]. A representative complex-type N-linked glycan is modeled on the basis of the structure of a glycan of human IgG1 (PDB 3AVE)[38]. The glycan core in the H_CA–gSV2C complex is green, and the remaining carbohydrates (mannose and NAG; gray) may potentially extend to the N-terminal subdomain of H_CA ($H_{CN}A$). $H_{CC}A$, C-terminal subdomain of H_CA.

interactions to SV2 recognition, which varied substantially among the eight different BoNT/A subtypes (**Supplementary Note 2**). In this regard, we mutated residues R1156 and R1294 of BoNT/A1 to their counterparts in other BoNT/A subtypes (for example, R1156E and R1294S), thereby disrupting their interactions with the peptide moiety of SV2C without affecting glycan binding. We used the double mutant H_CA T1145A T1146A as a control[10]. These two threonine residues, located at the core of the protein-protein interface, are conserved in all BoNT/A subtypes (**Supplementary Note 2**). We found that binding of H_CA T1145A T1146A to cultured rat hippocampal and cortical neurons was abolished (**Fig. 3a**,**b**). This result was consistent with the results of an earlier study showing that H_CA T1145A T1146A cannot bind to bSV2C[10]. Interestingly, we found that H_CA R1156E and R1294S still bound substantially to neurons (**Fig. 3a**,**b**), despite showing decreased binding to both human bSV2C and gSV2C *in vitro* (**Supplementary Fig. 5a–c**). These data suggest that loss of side chain–mediated interactions at R1156 and R1294 of BoNT/A1 is tolerated on neuronal surfaces, probably because of the presence of SV2 glycan and co-receptor gangliosides.

Glycan binding is essential for BoNT/A1's high potency

To further establish the physiological relevance of protein-glycan interactions, we produced full-length BoNT/A1 containing single-site glycan-binding-deficient mutations (F953G, F953R, H1064G, H1064R, G1292V, or G1292R) and examined their neurotoxicity at motor nerve terminals by using *ex vivo* mouse phrenic nerve hemidiaphragm (MPN) assays[19] (**Fig. 3f**). Remarkably, all of these mutations drastically decreased the potency of BoNT/A1. BoNT/A1 F953R had no detectable toxicity even at the maximal concentration tested (200 nM), thus it displayed a $>10^6$-fold reduction of neurotoxicity despite showing fully functional Zn^{2+} endoprotease activity *in vitro*. The mutation G1292R also severely decreased the toxicity, by 350-fold (ref. 20). Mutations H1064G and H1064R displayed three- and seven-fold decreases, respectively. These data demonstrate that glycan binding is essential for the high potency of BoNT/A1 at the motor nerve terminals, its physiological site of action.

The SV2 glycan-binding mode is conserved in BoNT/HA

We next examined whether glycan binding is conserved in natural variants of BoNT/A1, because BoNT genes have actively evolved, and at least 40 different subtypes of BoNT have been reported[21]. In this regard, we focused on a newly reported mosaic toxin type HA (BoNT/HA, also known as BoNT/FA), which has a hybrid-like structure including a BoNT/A1-like H_C[22–26]. H_CHA is highly similar to H_CA (~83% identical amino acids) (**Supplementary Note 2**). Sequence alignment revealed that most of the glycan-binding residues, such as F953 and H1064, are conserved in H_CA and H_CHA, but residues R1156 and R1294 of H_CA are M1148 and S1286 in H_CHA. H_CHA showed much weaker binding than H_CA to human bSV2C, whereas its binding to human gSV2C was comparable to that of H_CA (**Fig. 4a**). These results suggest that the loss of side chain interactions due to genetic changes of M1148 and S1286 in H_CHA is compensated by SV2C glycan. In contrast, H_CHA F943G (equivalent to H_CA F953G) did not bind to gSV2C in a pulldown assay, nor did it bind to cortical neurons, probably because of the disruption of glycan binding (**Fig. 4a**,**b**). These data confirm that a similar glycan-binding mode is conserved in H_CHA and is critical for its binding to SV2s on neurons.

Furthermore, we found that the SV2 glycan-binding residues are largely conserved in seven of the eight BoNT/A subtypes (BoNT/A1–A3 and A5–A8) identified to date[27] (**Supplementary Note 2**). Notably, BoNT/A4 is the only one with an arginine residue (R1292) at the equivalent position of BoNT/A1 G1292. Because the BoNT/A1 G1292R mutant drastically decreases BoNT/A1 toxicity by blocking its binding to SV2 glycan[20] (**Fig. 3** and **Supplementary Figs. 5** and **6**), we suggest that the disrupted glycan binding caused by residue R1292 is a major reason for the ~1,000-fold reduced biological activity of BoNT/A4 compared with that of BoNT/A1 (ref. 28). Together, our findings suggest that BoNT/A1 and variants use the genetically invariable carbohydrates as surrogate amino acids to engage the host receptors. Synergistic binding to two distinct cell-surface receptors, SV2 (including its peptide and glycan moieties) and ganglioside, provides a plausible explanation for the high potency of BoNT/A and its remarkable specificity for nerve terminals (**Fig. 4c**).

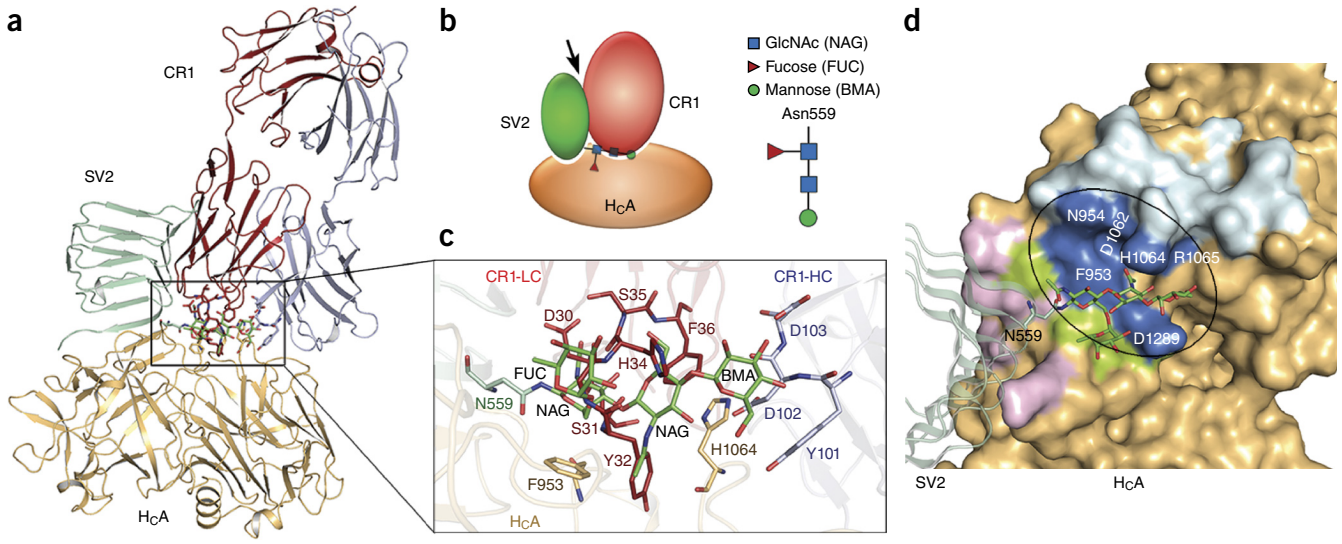

Figure 5 The SV2 glycan-binding site on BoNT/A1 is the target of the neutralizing antibody CR1. (**a**,**b**) BoNT/A1-neutralizing therapeutic antibody CR1 (PDB 2NYY)[29] occupies the SV2C glycan-binding site on H_CA but does not affect H_CA's SV2C peptide-binding site. The arrow in the schematic in **b** indicates the side-to-side clash between SV2C and CR1. (**c**) Close-up view of the interface. gSV2C N559 glycan (green), H_CA F953 and H1064 (gold), residues 30–36 of CR1 ligand chain (LC, red), and residues 101–103 of CR1 heavy chain (HC, gray) are shown in stick models. (**d**) Residues of H_CA that bind exclusively SV2C peptide, N559 glycan or CR1 are colored in purple, green, and cyan, respectively, and the H_CA residues that are contacted by both N559 glycan and CR1 are blue.

A new strategy for developing antibodies against BoNT/A

The new glycan receptor for BoNT/A presents a promising target for developing therapeutic toxin inhibitors. Remarkably, we found that a BoNT/A1-neutralizing human monoclonal antibody family, CR2/CR1, which is currently in clinical trials[29,30], directly targets the glycan-binding site on H_CA, such that the first antigen-binding loop of the light-chain variable region occupies the glycan-binding site (**Fig. 5a**). The key epitopes for CR2/CR1 include residues F953 and H1064 (ref. 29). Interestingly, residue F36 of CR2/CR1 uses a π-stacking interaction to bind BoNT/A1 H1064, mimicking its interactions with SV2C N559 glycan. CR2/CR1 also blocks binding of BoNT/A1 to bSV2C[20], but this effect is due to the large size of CR2/CR1 causing a side-to-side clash with bSV2C, because CR2/CR1 and bSV2C have nonoverlapping binding sites on H_CA (**Fig. 5b–d**). Together our data reveal that the strong neutralization potency of CR2/CR1 is empowered by simultaneously blocking BoNT/A1 binding to the glycan and peptide moieties of SV2.

DISCUSSION

Host cell-surface glycans are crucial for pathogen recognition. For example, the host range (e.g., swine, avian or human) of influenza hemagglutinins is largely dependent on carbohydrates [31]. Our results reveal a new host-recognition strategy by which pathogens simultaneously recognize a protein segment and the neighboring glycans as a composite binding site. This unique strategy uses a conserved post-translational modification as an evolutionarily static recognition site, in addition to protein-protein interactions that encode the location and specificity information. Together, this strategy provides a powerful solution to address the competing needs of achieving highly specific binding while also tolerating residue changes in receptors across multiple isoforms and species variants.

Intriguingly, a similar strategy may be used by some important broadly neutralizing human antibodies, which are capable of neutralizing multiple serotypes of targeted viruses, such as dengue viruses and HIV-1, by simultaneously recognizing the protein components and the highly conserved glycans on virus proteins[32–34]. A similar model has also recently been demonstrated for Notch1 receptor binding with its ligand Delta like 4 (DLL4)[35], such that DLL4 binds to the fucose and glucose at the base of an O-glycosylation site located within the protein-protein interface. Therefore, our findings offer a promising strategy for engineering ligand-receptor interactions and broadly neutralizing antibodies for therapeutic applications.

METHODS

Methods and any associated references are available in the online version of the paper.

Accession codes. Coordinates and structure factors for the H_CA–bSV2C and H_CA–gSV2C complexes have been deposited in the Protein Data Bank under accession codes PDB 5JMC and PDB 5JLV, respectively.

Note: Any Supplementary Information and Source Data files are available in the online version of the paper.

ACKNOWLEDGMENTS

This work was partly supported by National Institute of Allergy and Infectious Diseases (NIAID) grants R01AI091823 and R21AI123920 to R.J. and R01AI096169 to M.K.; by National Institute of Neurological Disorders and Stroke (NINDS) grant R01NS080833 to M.D.; and by Bundesministerium für Bildung und Forschung grants FK031A212A to A.R. and FK031A212B to B.G. Dorner (RKI). NE-CAT at the Advanced Photon Source (APS) is supported by a grant from the National Institute of General Medical Sciences (P41 GM103403). The Pilatus 6M detector at the 24-ID-C beamline is funded by a NIH-ORIP HEI grant (S10 RR029205). Use of the APS, an Office of Science User Facility operated for the US Department of Energy (DOE) Office of Science by Argonne National Laboratory, was supported by the US DOE under contract no. DE-AC02-06CH11357. We thank J. Weisemann for cloning H_CHA and N. Krez for dissecting the MPN hemidiaphragm tissue. We thank E. Chapman (University of Wisconsin–Madison), E. Johnson (University of Wisconsin–Madison), J. Marks (University of California, San Francisco), and R. Janz (The University of Texas Health Science Center at Houston) for generously providing reagents.

AUTHOR CONTRIBUTIONS

G.Y. and S.M. performed the cloning and mutagenesis. G.Y., K.L., and R.J. carried out the protein expression, purification, characterization, and crystallographic studies. K.P. collected the X-ray diffraction data. S.Z. and M.D. performed all experiments on cultured neurons. A.R. and S.M. generated the full-length BoNT/A1 mutants and performed the MPN assay. D.S., K.B., and M.K. performed the SPR studies. R.J., M.D., and A.R. wrote the manuscript with input from other authors.

COMPETING FINANCIAL INTERESTS

The authors declare no competing financial interests.

1. Montecucco, C. How do tetanus and botulinum neurotoxins bind to neuronal membranes? *Trends Biochem. Sci.* **11**, 314–317 (1986).
2. Montecucco, C., Rossetto, O. & Schiavo, G. Presynaptic receptor arrays for clostridial neurotoxins. *Trends Microbiol.* **12**, 442–446 (2004).
3. Rummel, A. Double receptor anchorage of botulinum neurotoxins accounts for their exquisite neurospecificity. *Curr. Top. Microbiol. Immunol.* **364**, 61–90 (2013).
4. Dong, M. *et al.* SV2 is the protein receptor for botulinum neurotoxin A. *Science* **312**, 592–596 (2006).
5. Mahrhold, S., Rummel, A., Bigalke, H., Davletov, B. & Binz, T. The synaptic vesicle protein 2C mediates the uptake of botulinum neurotoxin A into phrenic nerves. *FEBS Lett.* **580**, 2011–2014 (2006).
6. Dong, M. *et al.* Glycosylated SV2A and SV2B mediate the entry of botulinum neurotoxin E into neurons. *Mol. Biol. Cell* **19**, 5226–5237 (2008).
7. Peng, L., Tepp, W.H., Johnson, E.A. & Dong, M. Botulinum neurotoxin D uses synaptic vesicle protein SV2 and gangliosides as receptors. *PLoS Pathog.* **7**, e1002008 (2011).
8. Rummel, A. *et al.* Botulinum neurotoxins C, E and F bind gangliosides via a conserved binding site prior to stimulation-dependent uptake with botulinum neurotoxin F utilising the three isoforms of SV2 as second receptor. *J. Neurochem.* **110**, 1942–1954 (2009).
9. Fu, Z., Chen, C., Barbieri, J.T., Kim, J.J. & Baldwin, M.R. Glycosylated SV2 and gangliosides as dual receptors for botulinum neurotoxin serotype F. *Biochemistry* **48**, 5631–5641 (2009).
10. Benoit, R.M. *et al.* Structural basis for recognition of synaptic vesicle protein 2C by botulinum neurotoxin A. *Nature* **505**, 108–111 (2014).
11. Chai, Q. *et al.* Structural basis of cell surface receptor recognition by botulinum neurotoxin B. *Nature* **444**, 1096–1100 (2006).
12. Jin, R., Rummel, A., Binz, T. & Brunger, A.T. Botulinum neurotoxin B recognizes its protein receptor with high affinity and specificity. *Nature* **444**, 1092–1095 (2006).
13. Janz, R. & Südhof, T.C. SV2C is a synaptic vesicle protein with an unusually restricted localization: anatomy of a synaptic vesicle protein family. *Neuroscience* **94**, 1279–1290 (1999).
14. Helenius, A. & Aebi, M. Intracellular functions of N-linked glycans. *Science* **291**, 2364–2369 (2001).
15. Rummel, A., Mahrhold, S., Bigalke, H. & Binz, T. The H_{CC}-domain of botulinum neurotoxins A and B exhibits a singular ganglioside binding site displaying serotype specific carbohydrate interaction. *Mol. Microbiol.* **51**, 631–643 (2004).
16. Pirazzini, M., Rossetto, O., Bolognese, P., Shone, C.C. & Montecucco, C. Double anchorage to the membrane and intact inter-chain disulfide bond are required for the low pH induced entry of tetanus and botulinum neurotoxins into neurons. *Cell. Microbiol.* **13**, 1731–1743 (2011).
17. Swiech, K., Picanço-Castro, V. & Covas, D.T. Human cells: new platform for recombinant therapeutic protein production. *Protein Expr. Purif.* **84**, 147–153 (2012).
18. Croset, A. *et al.* Differences in the glycosylation of recombinant proteins expressed in HEK and CHO cells. *J. Biotechnol.* **161**, 336–348 (2012).
19. Bigalke, H. & Rummel, A. Botulinum neurotoxins: qualitative and quantitative analysis using the mouse phrenic nerve hemidiaphragm assay (MPN). *Toxins (Basel)* **7**, 4895–4905 (2015).
20. Strotmeier, J. *et al.* Identification of the synaptic vesicle glycoprotein 2 receptor binding site in botulinum neurotoxin A. *FEBS Lett.* **588**, 1087–1093 (2014).
21. Rossetto, O., Pirazzini, M. & Montecucco, C. Botulinum neurotoxins: genetic, structural and mechanistic insights. *Nat. Rev. Microbiol.* **12**, 535–549 (2014).
22. Barash, J.R. & Arnon, S.S. A novel strain of *Clostridium botulinum* that produces type B and type H botulinum toxins. *J. Infect. Dis.* **209**, 183–191 (2014).
23. Gonzalez-Escalona, N. *et al.* Draft genome sequence of bivalent *Clostridium botulinum* strain IBCA10-7060, encoding botulinum neurotoxin B and a new FA mosaic type. *Genome Announc.* **2**, e01275–14 (2014).
24. Kalb, S.R. *et al.* Functional characterization of botulinum neurotoxin serotype H as a hybrid of known serotypes F and A (BoNT F/A). *Anal. Chem.* **87**, 3911–3917 (2015).
25. Maslanka, S.E. *et al.* A novel Botulinum toxin, previously reported as serotype H, has a hybrid structure of known serotypes A and F that is neutralized with serotype A antitoxin. *J. Infect. Dis.* **213**, 379–385 (2016).
26. Fan, Y. *et al.* Immunological characterization and neutralizing ability of monoclonal antibodies directed against botulinum neurotoxin type H. *J. Infect. Dis.* **213**, 1606–1614 (2016).
27. Kull, S. *et al.* Isolation and functional characterization of the novel *Clostridium botulinum* neurotoxin A8 subtype. *PLoS One* **10**, e0116381 (2015).
28. Whitemarsh, R.C. *et al.* Characterization of botulinum neurotoxin A subtypes 1 through 5 by investigation of activities in mice, in neuronal cell cultures, and *in vitro*. *Infect. Immun.* **81**, 3894–3902 (2013).
29. Garcia-Rodriguez, C. *et al.* Molecular evolution of antibody cross-reactivity for two subtypes of type A botulinum neurotoxin. *Nat. Biotechnol.* **25**, 107–116 (2007).
30. Nayak, S.U. *et al.* Safety and pharmacokinetics of XOMA 3AB, a novel mixture of three monoclonal antibodies against botulinum toxin A. *Antimicrob. Agents Chemother.* **58**, 5047–5053 (2014).
31. Skehel, J.J. & Wiley, D.C. Receptor binding and membrane fusion in virus entry: the influenza hemagglutinin. *Annu. Rev. Biochem.* **69**, 531–569 (2000).
32. Rouvinski, A. *et al.* Recognition determinants of broadly neutralizing human antibodies against dengue viruses. *Nature* **520**, 109–113 (2015).
33. Garces, F. *et al.* Structural evolution of glycan recognition by a family of potent HIV antibodies. *Cell* **159**, 69–79 (2014).
34. Kong, L. *et al.* Supersite of immune vulnerability on the glycosylated face of HIV-1 envelope glycoprotein gp120. *Nat. Struct. Mol. Biol.* **20**, 796–803 (2013).
35. Luca, V.C. *et al.* Structural biology: structural basis for Notch1 engagement of Delta-like 4. *Science* **347**, 847–853 (2015).
36. Laskowski, R.A. & Swindells, M.B. LigPlot+: multiple ligand-protein interaction diagrams for drug discovery. *J. Chem. Inf. Model.* **51**, 2778–2786 (2011).
37. Stenmark, P., Dupuy, J., Imamura, A., Kiso, M. & Stevens, R.C. Crystal structure of botulinum neurotoxin type A in complex with the cell surface co-receptor GT1b-insight into the toxin-neuron interaction. *PLoS Pathog.* **4**, e1000129 (2008).
38. Matsumiya, S. *et al.* Structural comparison of fucosylated and nonfucosylated Fc fragments of human immunoglobulin G1. *J. Mol. Biol.* **368**, 767–779 (2007).

ONLINE METHODS

No statistical method was used to predetermine sample size. The experiments were not randomized and were not performed with blinding to the conditions of the experiments.

Construct design and cloning. The gene encoding H_CA (residues N872–L1296) was cloned into the expression vector pQE30 with an N-terminal His_6 tag and a PreScission protease–cleavage site. H_CHA (residues E860–L1286) was cloned into the pGEX-4T-2 vector, which has a thrombin-cleavage site after GST. The core region of human SV2C-L4 (residues V473–T567) was cloned into two different vectors: pET28a for *E. coli* expression and pcDNA for mammalian cell expression. For *E. coli* expression, a His_6-SUMO (*Saccharomyces cerevisiae* Smt3p) tag was introduced at the N terminus of SV2C-L4 to facilitate protein expression and purification (SUMO-bSV2C). For mammalian cell expression, a human IL2 signal sequence (MYRMQLLSCIALSLALVTNS), a His_9 tag, and a factor Xa–cleavage site were added to the N terminus of SV2C-L4 (gSV2C). A second SV2C mammalian expression construct was made on the basis of gSV2C by inserting SUMO between the factor Xa site and SV2C (SUMO-gSV2C). Rat SV2C-L4 (residues P455–Y577) was covalently linked to the C terminus of H_CA through a peptide linker composed of a thrombin-cleavage site (LVPRGS) and a PreScission protease–cleavage site (LEVLFQGP), and the covalently linked H_CA and rat bSV2C (H_CA–bSV2C) was cloned into pET28a with an N-terminal His_6 tag and a thrombin-cleavage site. All H_CA and H_CHA mutations were generated with QuikChange site-directed mutagenesis (Agilent). All pH6tBoNTA mutants were prepared with the GeneTailor method (Invitrogen), with suitable primers and pH6tBoNTA as the template DNA[20].

Protein expression and purification. H_CA, H_CHA, SUMO-bSV2C, and H_CA–bSV2C were expressed in *E. coli* strain BL21 Star (DE3) (Invitrogen). Bacteria were cultured at 37 °C in LB medium containing appropriate selecting antibiotics. The temperature was reduced to 18 °C when the OD_{600} reached 0.4. Expression was induced with 0.2 mM IPTG when the OD_{600} reached 0.7, and growth was allowed to continue at 18 °C for ~16 h. The cells were harvested by centrifugation and stored at −80 °C until use.

WT and mutated recombinant full-length neurotoxin H6tBoNTA were produced under biosafety level 2 containment (project number GAA A/Z 40654/3/123) with the *E. coli* strain M15pREP4 (Qiagen) during 16 h of induction at 22 °C in the presence of 0.2 mM IPTG and were purified on Co^{2+}–Talon matrix (Takara Bio Europe). Full-length neurotoxins were eluted with 50 mM Tris-HCl, pH 8.0, 150 mM NaCl, and 250 mM imidazole, subjected to size-exclusion chromatography (SEC; Superdex-200 16/60 column, GE Healthcare) in 100 mM Tris-HCl, pH 8.0, and 150 mM NaCl, frozen in liquid nitrogen and kept at −70 °C.

The histidine-tagged proteins (H_CA, SUMO-bSV2C, and H_CA–bSV2C) were purified with Ni^{2+}–NTA (Qiagen) affinity resins in a buffer containing 50 mM Tris, pH 8.0, 400 mM NaCl, and 40 mM imidazole. The proteins were eluted with a high-imidazole buffer (50 mM Tris, pH 8.0, 400 mM NaCl, and 300 mM imidazole) and then dialyzed at 4 °C against a buffer containing 20 mM HEPES, pH 7.5, and 150 mM NaCl. The histidine tag of H_CA and the His_6-SUMO tag of SUMO-bSV2C were cleaved by PreScission and SUMO proteases, respectively. For the covalently linked H_CA–bSV2C, both thrombin and PreScission protease were used to cut the linker between the two proteins to avoid potential conformational constraint. GST-H_CHA fusion protein was purified with glutathione Sepharose 4B affinity resin (GE Healthcare) in a buffer containing 20 mM HEPES, pH 7.5, and 150 mM NaCl. H_CHA was then released from the resins by on-column cleavage with thrombin.

Tag-cleaved H_CA and H_CHA were further purified by MonoS ion-exchange chromatography (GE Healthcare) in a buffer containing 50 mM MES, pH 6.0, and eluted with a NaCl gradient. The peak fractions were then subjected to Superdex-200 SEC (GE Healthcare) in a buffer containing 20 mM sodium phosphate, pH 6.0, and 50 mM NaCl. SUMO-bSV2C (with the His_6-SUMO tag cleaved or uncleaved) and cleaved H_CA–bSV2C were further purified by Superdex-200 SEC in a buffer containing 20 mM HEPES, pH 7.5, and 150 mM NaCl. The H_CA–bSV2C complex was concentrated to ~2 mg/ml for crystallization.

SUMO-gSV2C and gSV2C were expressed and secreted from HEK 293 cells (BioLegend) and purified directly from cell culture medium with Ni^{2+}–NTA. The proteins were eluted from the resins with a high concentration of imidazole and dialyzed against a buffer containing 50 mM Tris, pH 8.0, and 400 mM NaCl. gSV2C was then mixed with the purified H_CA at a molar ratio of ~1:2, and the H_CA–gSV2C complex was isolated with Ni^{2+}–NTA resin. After dialysis against a buffer containing 20 mM HEPES, pH 7.5, and 150 mM NaCl, the complex was further purified by Superdex-200 SEC with the same buffer. The complex was concentrated to ~10 mg/ml for crystallization.

Crystallization. Initial crystallization screens were carried out with a Gryphon crystallization robot (Art Robbins Instruments) with high-throughput crystallization screening kits (Hampton Research and Qiagen). Extensive manual optimization was then performed at 20 °C with the hanging-drop vapor-diffusion method when proteins were mixed with reservoir solutions in 1:1 ratio. The H_CA–bSV2C complex was initially crystallized in a condition containing 100 mM sodium cacodylate, pH 6.5, 13% polyethylene glycol (PEG) 3350, and 200 mM NaCl. The best crystals were obtained in the presence of 0.7% (v/v) 1-butanol, which was identified with an additive screen kit (Hampton Research). The crystals were cryoprotected in the original mother liquor supplemented with 20% (v/v) glycerol and flash frozen in liquid nitrogen. The H_CA–gSV2C complex was originally crystallized as thin plates in a condition composed of 100 mM sodium acetate, pH 4.6, 20% PEG 3350, and 200 mM ammonium phosphate monobasic. These crystals diffracted poorly. After extensive additive screening and optimization, the best crystals were obtained in the presence of 4% (w/v) polypropylene glycol P 400. The crystals were cryoprotected in the reservoir solution supplemented with 20% (v/v) ethylene glycol and flash frozen in liquid nitrogen.

Data collection and structure determination. The X-ray diffraction data were collected at 100 K at the NE-CAT beamline 24-ID, Advanced Photon Source (APS). The data were processed with XDS[39]. The structure of H_CA–bSV2C was determined with Phaser molecular replacement software[40] with the structure of H_CA (PDB 3FUO)[9] as the search model. The structural model of bSV2C was manually built, and the structural modeling and refinement were carried out iteratively with COOT[41] and Refmac from the CCP4 suite[42]. This structure was later used as the search model to determine the structure of the H_CA–gSV2C complex. All refinement progress was monitored with the R_{free} value with a 5% randomly selected test set[43]. The structures were validated through the MolProbity web server[44] and showed excellent stereochemistry. Data collection and structural refinement statistics are listed in **Table 1**. All structure figures were prepared with PyMOL (http://www.pymol.org/).

Pulldown assays. Pulldown assays were performed with Ni^{2+}–NTA resin in 1 ml buffer containing 50 mM Tris, pH 8.0, 400 mM NaCl, 10 mM imidazole, and 0.1% Tween-20. SUMO-bSV2C or gSV2C served as the bait, and H_CA or H_CHA variants served as the prey. SV2C was preincubated with Ni^{2+}–NTA resin at 4 °C for 1 h, and the unbound protein was washed away. The resin was then divided into small aliquots (~5 μg of bait) and mixed with the prey (~30 μg). Pulldown assays were carried out at 4 °C for ~1.5 h. The resin was washed twice, and the bound proteins were released from the resin with 300 mM imidazole.

Protein melting assay. The thermal stability of H_CA or H_CHA variants was measured with a fluorescence-based thermal shift assay on a StepOne real-time PCR machine (Life Technologies). The protein (~5 μM) was mixed with the fluorescent dye SYPRO Orange (Sigma-Aldrich) immediately before the experiment. The samples were heated from 25 °C to 90 °C over ~45 min. The midpoint of the protein-melting curve (T_m) was determined with the analysis software provided by the instrument manufacturer. Data obtained from three independent experiments were averaged to generate the bar graph.

Surface plasmon resonance (SPR). Binding kinetics and affinity were determined on a Biacore X100 unit (GE Healthcare) at 25 °C with HBS-EP+ (10 mM HEPES, pH 7.4, 150 mM NaCl, 3 mM EDTA, and 0.05% Tween-20) as running buffer at a flow rate of 30 μL/min. With standard EDC/NHS amine coupling chemistry, SUMO-gSV2C or SUMO-bSV2C were coupled on flow cell (Fc) 2 of a CM5 sensor chip (GE Healthcare) to a surface density of ~83 resonance units (RUs) or ~105 RUs, respectively. Fc1 was used as a blank control and was immobilized by EDC/NHS activation before blocking with 1 M ethanolamine (GE Healthcare).

For kinetic measurements, H_CA was injected in 1:3 dilution series ranging from 1,200 nM to 4.94 nM for gSV2C or 2,000 nM to 2.74 nM for bSV2C. Each

measurement started and ended with injection of the highest analyte concentration to ensure retained binding capacity. Association was monitored for 120 s after analyte injection, and this was followed by 300-s injections of running buffer to monitor binding dissociation. Between measurements, the surface was regenerated with 60-s injections of 10 mM glycine-HCl, pH 1.7, at 10 µL/min. Binding kinetics was determined by fitting the double referenced[45] binding curves with the heterogeneous (gSV2C) or the 1:1 Langmuir binding models (bSV2C) with global R_{max}, with RI set to zero (Biacore Evaluation Software 2.01). Owing to the highly transient interaction of H_CA with bSV2C, equilibrium binding was reached for all H_CA concentrations tested. Therefore, steady-state affinity was determined for bSV2C by fitting a four-parametric Hill equation to the binding responses 65 s after analyte injection over log-transformed H_CA concentrations with Prism 5.04 (GraphPad), with the bottom constraint set to zero. The good agreement between the binding affinity determined by kinetic analysis, and the steady-state affinity proved that the kinetic binding rates for bSV2C were reliable despite being close to the measurement limits of the instrument. Kinetic binding rates were determined in $n = 2$ (bSV2C) or $n = 3$ (gSV2C) independent experiments. The values are shown as the mean ± s.d.

To compare the interaction of H_CA WT and its mutants with bSV2C (511 RUs) and separately with gSV2C (479 RUs), the reactions were performed in 'interactive manual run mode'. The H_CA variants were injected at concentrations of 0.01, 1.0, 10, 25, 50, 75, 100, and 200 nM, each in triplicate, and at a flow rate of 10 µL/min. The chip surface was regenerated by two injections of glycine-HCl (10 mM, pH 2.0, 30-s contact time) thus allowing the removal of the analyte without changing the activity of the immobilized ligand. The activity was confirmed on the basis of the equal responses obtained from the binding assays before and after regeneration. Results were plotted as response (RU) versus concentration of H_CA with Prism 6 (GraphPad Software).

Cell biology materials and constructs. *Sv2a*- and *Sv2b*-knockout mice (strain B6;129P2-*Sv2a*^{tm1Sud} *Sv2b*^{tm1Sud}/J) were obtained from the Jackson Laboratory. Rat cDNAs encoding SV2A, SV2B, and SV2C were generously provided by R. Janz. They were cloned into a lentiviral vector (Lox-Syn-Syn) as previously described[7]. This vector contains two separate neuronal-specific synapsin promoters. One promoter drives expression of SV2, and the other drives expression of GFP as a marker. Human cDNA encoding SV2C was obtained from the PlasmID repository of the Harvard Medical School. Human monoclonal antibody against H_CA (RAZ-1) was generously provided by J. Marks. Mouse monoclonal antibodies against VAMP2 (Cl 69.1), SNAP-25 (Cl 71.2), and Syp (Cl 7.2) were generously provided by E. Chapman and are available from Synaptic Systems. SV2 (pan-SV2) was also provided by E. Chapman, and it is available from The Developmental Studies Hybridoma Bank (AB2315387). The following antibodies were purchased from indicated vendors: mouse monoclonal antibody against β-actin (Sigma, A2228); rabbit polyclonal antibody against synapsin (Millipore, Ab1543p); chicken polyclonal antibody against GFP (Aves Labs, GFP-1020). Antibody validation is available on the manufacturers' websites. Purified BoNT/A1 from the Hall-A strain and BoNT/D from the D1873 strain were generously provided by E. Johnson.

Neuron culture and lentivirus transduction. Rat hippocampal and cortical neurons were prepared from E18–19 embryos dissected from pregnant rats (Sprague Dawley strain, purchased from Charles River). Mouse SV2A/B double-knockout neurons were prepared from postnatal day 1 pups as previously described[7]. Dissected hippocampi and cortex were dissociated with papain, per the manufacturer's instructions (Worthington Biochemical). Cells were plated on poly-D-lysine–coated coverslips. Experiments were carried out generally with DIV (days *in vitro*) 13–15 neurons. Lentiviruses were prepared as described previously with HEK293FT cells[7]. Viruses were added to neurons at DIV5.

H_CA and H_CHA binding to neurons. Neurons were exposed to 100 nM H_CA or H_CHA in high-K^+ buffer containing 87 mM NaCl, 56 mM KCl, 1.5 mM KH_2PO_4, 8 mM Na_2HPO_4, 0.5 mM $MgCl_2$, and 1 mM $CaCl_2$, for 5 min at 37 °C. Cells were then washed three times with phosphate-buffered saline (PBS). Binding of H_CA or H_CHA was examined with two complementary approaches. (i) For immunostaining, neurons were fixed with 4% paraformaldehyde and permeabilized with 0.3% Triton X-100 in PBS solution. Images were collected with a Leica TCS SP8 confocal microscope with a 40× oil objective. At least three representative images were collected per condition. (2) For immunoblot analysis, neurons were harvested in a lysis buffer (PBS with 1% Triton X-100, 0.05% SDS and protease-inhibitor cocktail (Roche), 100 µL per well in 24-well plates). Lysates were centrifuged for 10 min at 4 °C, and the supernatants were subjected to SDS–PAGE and western blot analysis. Binding of H_CA or H_CHA was detected with a monoclonal human anti-H_CA antibody (RAZ-1)4, which recognizes both H_CA and H_CHA. It also recognizes mutants of H_CA and H_CHA examined in this study with similar sensitivity (input lanes in **Figs. 3b** and **4b**). All experiments were repeated three times independently.

Entry of BoNTs into neurons. Neurons were exposed to 1 nM BoNT/A1 and 0.1 nM BoNT/D in high-K^+ buffer for 5 min at 37 °C. Cells were washed three times with PBS and further incubated in toxin-free medium for 8 h. Neuron lysates were then harvested and subjected to immunoblot analysis to detect cleavage of the toxin substrates SNAP-25 (for BoNT/A1) and VAMP2 (for BoNT/D). Cleavage of SNAP-25 by BoNT/A1 generates a smaller fragment that can be detected on immunoblots. Cleavage of VAMP2 by BoNT/D resulted in a loss of immunoblot signal of VAMP2. All experiments were repeated three times independently.

Mouse phrenic nerve hemidiaphragm (MPN) assays. The MPN assays were performed as described previously, with ~4- to 6-week-old female NMRI mice weighing 20–30 g (Janvier SA)[19,20]. According to German animal protection law (TSchG §4 Abs. 3, killing of animals for scientific purposes), animals were sacrificed by trained personnel before dissection of organs, and numbers were reported annually to the animal welfare officer of the Central Animal Laboratory and to the local authority, Veterinäramt Hannover. First, mice were euthanized by CO_2 anesthesia and were subsequently exsanguinated via an incision of the ventral aspect of the throat. The chest of each mouse was opened, and the phrenic nerve hemidiaphragm tissue was explanted and placed into an organ bath. The phrenic nerve was continuously stimulated at 5–25 mA with a frequency of 1 Hz and with a 0.1-ms pulse duration. Isometric contractions were transformed with a force transducer and recorded with VitroDat Online software (FMI). The time required to decrease the amplitude to 50% of the starting value (paralytic half-time) was determined. To allow comparison of the altered neurotoxicity of mutants with WT H6tBoNTA, a power function ($y(H6tBoNTA; 10, 30, 80\ pM) = 139.6\times^{-0.1957}$, $R^2 = 0.9991$) was fitted to a concentration–response curve consisting of three concentrations determined in 3–6 technical replicates. The resulting paralytic half-times of the H6tBoNTA mutants were converted to concentrations of the WT with the above power functions and were finally expressed as relative neurotoxicity.

39. Kabsch, W. Xds. *Acta Crystallogr. D Biol. Crystallogr.* **66**, 125–132 (2010).
40. McCoy, A.J. *et al.* Phaser crystallographic software. *J. Appl. Crystallogr.* **40**, 658–674 (2007).
41. Emsley, P. & Cowtan, K. Coot: model-building tools for molecular graphics. *Acta Crystallogr. D Biol. Crystallogr.* **60**, 2126–2132 (2004).
42. Potterton, E., Briggs, P., Turkenburg, M. & Dodson, E. A graphical user interface to the CCP4 program suite. *Acta Crystallogr. D Biol. Crystallogr.* **59**, 1131–1137 (2003).
43. Brünger, A.T. Free R value: a novel statistical quantity for assessing the accuracy of crystal structures. *Nature* **355**, 472–475 (1992).
44. Chen, V.B. *et al.* MolProbity: all-atom structure validation for macromolecular crystallography. *Acta Crystallogr. D Biol. Crystallogr.* **66**, 12–21 (2010).
45. Myszka, D.G. Improving biosensor analysis. *J. Mol. Recognit.* **12**, 279–284 (1999).

doi:10.1038/nsmb.3245